

Photoexcitation of NO<sub>2</sub> in He<sub>n</sub> Droplets above the Gas-Phase Dissociation Threshold<sup>†</sup>

D. Stolyarov, E. Polyakova, and C. Wittig\*

Department of Chemistry, University of Southern California, Los Angeles, California 90089

Received: April 23, 2004; In Final Form: July 13, 2004

The guest–host dynamics of NO<sub>2</sub> embedded in He<sub>n</sub> droplets have been examined by recording depletion spectra of mass spectrometer signals at  $m/z$  values of 8 (He<sub>2</sub><sup>+</sup>), 30 (NO<sup>+</sup>), and 46 (NO<sub>2</sub><sup>+</sup>) throughout the wavelength range 340–402 nm. At energies above the  $\tilde{A}/\tilde{X}$  conical intersection, gas-phase NO<sub>2</sub> is known to exhibit quantum chaos, and it is also known that deactivation of embedded NO<sub>2</sub> by the helium host is efficient in this regime. Above the gas-phase dissociation threshold ( $D_0$ ) it is shown that there is no *net* unimolecular decomposition all the way up to  $D_0 + 4300$  cm<sup>-1</sup>. At the upper end of this range, gas-phase NO<sub>2</sub> decomposes with rate coefficients whose values are  $\sim 5 \times 10^{12}$  s<sup>-1</sup>, which is expected to be larger than the deactivation rates in liquid helium. The deactivation rate in the quantum-chaotic region 17 700–18 300 cm<sup>-1</sup> was found previously to be  $\sim 1.4 \times 10^{12}$  s<sup>-1</sup>, and it is expected that this will increase at yet higher energies, but not exceed  $5 \times 10^{12}$  s<sup>-1</sup>. To within the experimental uncertainty, it is found that reaction products do not leave the droplets. This is attributed to efficient relaxation and (at the highest energies examined) recombination within the droplets. On the basis of these results, it is concluded that small polyatomics embedded in He<sub>n</sub> droplets that have  $\langle n \rangle$  values of  $\sim 10^4$  or larger will not undergo *net* unimolecular reaction if the gas-phase pathway is barrierless, with two possible exceptions: (i) if one or both of the products has a positive chemical potential and (ii) if the scattering cross section of the product(s) with helium is small.

## Introduction

The photophysics and photochemistry of molecules and clusters embedded in/on superfluid helium nanodroplets continues to receive a great deal of attention. These droplets, hereafter denoted He<sub>n</sub>, where  $n$  is the number of helium atoms in the droplet, are said to provide ideal matrixes for isolating molecules and small aggregates and studying a broad range of fundamental interactions.<sup>1–5</sup> The interactions can be intramolecular within a single dopant molecule, intermolecular between dopant species (e.g., molecule–molecule, molecule–atom), between one or more dopant species and the helium host, or combinations of the above.

The He<sub>n</sub> droplets act as benign matrixes in many respects. They are composed of a 0.4 K superfluid quantum liquid that resides in essentially its ground state. For doped clusters in their native states, the dopant–host interactions are among the weakest in nature. Thus, for many purposes, there can be no better-characterized matrix host than superfluid helium droplets.

Photoexcitation of the dopant can alter dramatically this tranquil situation by introducing strong interactions. For example, the electrophobic nature of helium wreaks havoc with excitations that transfer electron density toward the outer reaches of the chromophore, in effect expanding its size and leading to large blue shifts in ultraviolet absorption spectra.<sup>1</sup> Moreover, vigorous and complex intramolecular vibrational dynamics and their associated dopant–host interactions do not perceive of the host as being merely a quiescent fluid. Rather, in this case, the helium responds as an ensemble of particles, akin to a dense gas, and average line widths of  $\sim 7$  cm<sup>-1</sup> fwhm have been recorded in absorption spectra of NO<sub>2</sub> embedded in He<sub>n</sub>.<sup>6</sup> In the quantum liquid, these line widths are homogeneous, so they correspond to subpicosecond deactivation times, which is hardly

a small effect. These studies were carried out in the energy range 17 700–18 300 cm<sup>-1</sup>, where it is known that strong nonadiabatic interaction via conical intersection of the  $\tilde{X}$  and  $\tilde{A}$  adiabats yields manifolds of A<sub>1</sub> and B<sub>2</sub> vibronic symmetries, each of which can be said to be quantum chaotic.<sup>7,8</sup> Though this spectrum was reported earlier,<sup>6</sup> as it is central to the interpretation of the results presented below, it is given here as Figure 1.

It is not difficult to appreciate that vibrational relaxation in the regime of quantum chaos can be efficient. Sensitivity to initial conditions and the associated divergence of nearby trajectories—a signature effect in chaotic classical systems—suggests a sensitivity to perturbation that is manifest as efficient relaxation of resolved levels of quantum-chaotic manifolds. This scenario differs qualitatively from that of low-lying vibrational levels, such as one or two quanta of a normal or local mode. These cases are usually characterized by relatively slow vibrational relaxation, as evidenced, for example, by narrow spectral line widths.<sup>9</sup>

Referring to Figure 1, though the broad line widths indicate efficient relaxation, the average amounts of energy lost by each of the levels is unknown. We believe that there is no mode specificity. In the regime of quantum chaos, the levels can be described as random mixtures of any vibrational basis that is derived from a separable Hamiltonian, and perturbation by the helium transfers excitation among such levels with good efficiency, in accord with the sensitivity to perturbation in the regime of quantum chaos.

It is not surprising that the spectrum shown in Figure 1 can be fit reasonably well by using a width of 7 cm<sup>-1</sup> for *each* of the levels, as well as a shift to higher energies of 7 cm<sup>-1</sup> for *each* of the levels. Namely, the randomness mentioned above results in each of the widths having roughly the same value, and likewise for the shifts. As the energy is increased from  $\sim 18\,000$  cm<sup>-1</sup> to the gas-phase photodissociation threshold,  $D_0 = 25\,128.5$  cm<sup>-1</sup>,<sup>10</sup> the density of states increases and the

<sup>†</sup> Part of the special issue “Tomas Baer Festschrift”.

\* Corresponding author. E-mail: wittig@usc.edu.

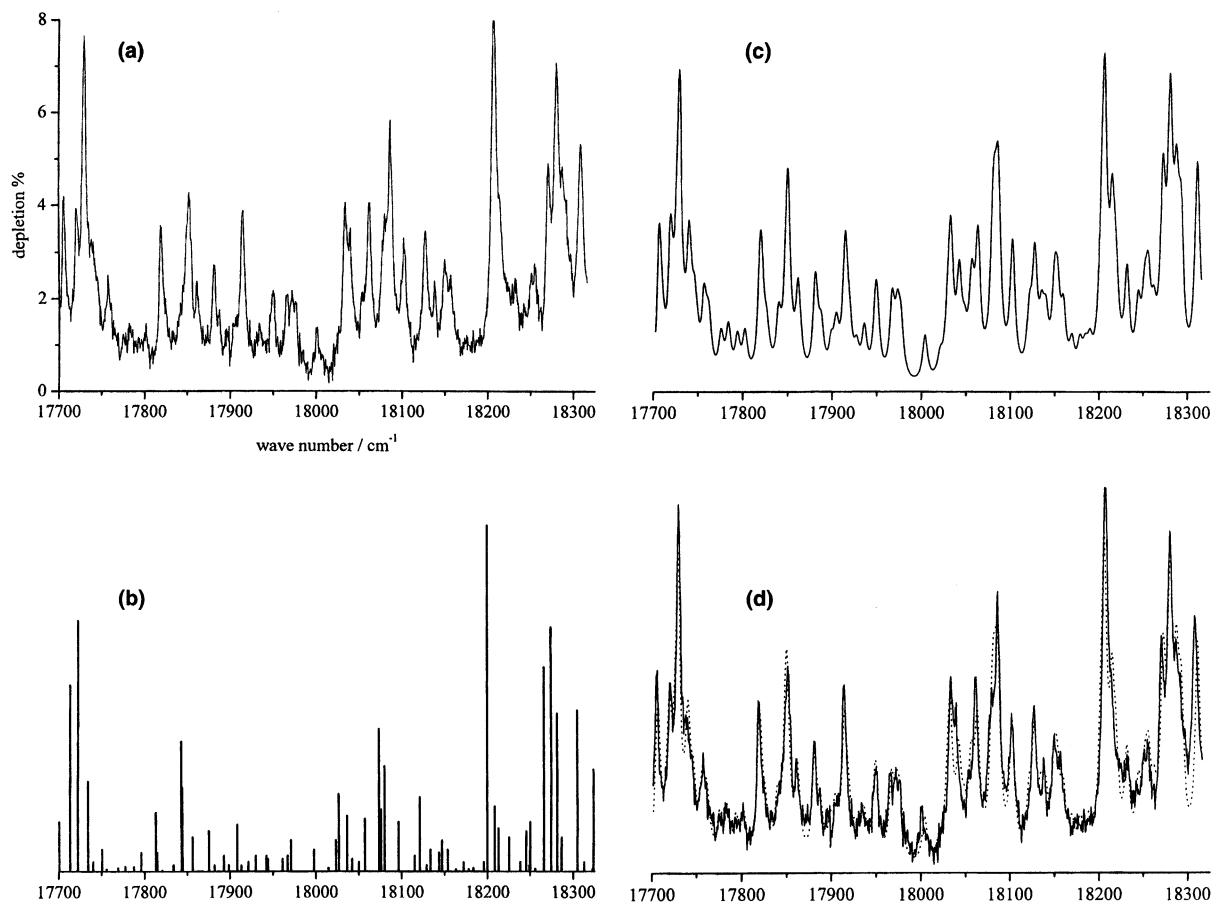


**Figure 1.** (a) Mass spectrometer depletion spectrum recorded at  $m/z = 30$ . (b) Frequencies and intensities of  $R_0$  lines recorded by using LIF are taken from Georges et al.<sup>7</sup> (c) All of the lines in (b) have been assigned  $7 \text{ cm}^{-1}$  widths and blue-shifted by  $7 \text{ cm}^{-1}$ . The intensities are fitted to the experimental spectrum. (d) Experimental and simulated spectra are overlapped.

intramolecular dynamics become more vigorous. Thus, spectral congestion is inevitable.

The general scientific issue of photoinitiated unimolecular decomposition in  $\text{He}_n$  nanodroplets remains open. The physical content of this dissociation mechanism differs qualitatively from that of direct photodissociation. With direct photodissociation, fragments are thrust apart forcefully on a short time scale (typically  $< 100 \text{ fs}$ ), and a high percentage of the available energy appears as interfragment exit channel repulsion along the reaction coordinate. This has been examined recently for  $\text{CH}_3\text{I}$  in  $\text{He}_n$  by Drabbels.<sup>11</sup> He reports that both  $\text{CH}_3$  and  $\text{I}(^2\text{P}_{3/2})$  enter the gas phase following the photodissociation of  $\text{CH}_3\text{I}$  embedded in  $\text{He}_n$ , with the iodine atom being caged more effectively than the  $\text{CH}_3$ . Along similar lines, Kanaev et al. have excited  $\text{H}_2\text{O}$  in  $\text{He}_n$  at short wavelengths (40–140 nm).<sup>12</sup> They report fluorescence from several electronically excited dissociation products, and they note that ionization is suppressed relative to dissociation, which is not surprising, given that the electron must be ejected through a sea of helium.

In contrast to direct photodissociation, in the case of unimolecular decomposition, the molecule's intramolecular vibrational dynamics ensue prior to dissociation, and this excitation can be coupled strongly to the host medium. This presents an obvious question: given the competition between vibrational relaxation and unimolecular decomposition, what are their respective efficacies, and how does dissociation, if it occurs at all, vary with energy?

In the experiments described below, we have examined the photoexcitation, in  $\text{He}_n$  droplets, of an embedded molecule that is known to undergo photoinitiated unimolecular decomposition

in the gas phase over a broad range of photon energies, namely,  $\text{NO}_2$ . The  $\text{NO}_2$  molecule is an especially attractive candidate for such a study because it places at our disposal a wealth of knowledge about its gas-phase photochemistry, as well as its relaxation in  $\text{He}_n$  in the regime of vibronic chaos.<sup>6</sup> In addition, it provides access to the largest possible gas-phase reaction rate coefficients that are consistent with a unimolecular decomposition mechanism, i.e.,  $k_{\text{uni}}$  values as high as  $\sim 5 \times 10^{12} \text{ s}^{-1}$ .<sup>13</sup> With larger rate coefficients, it is unreasonable to assume that intramolecular vibrational redistribution (IVR) proceeds much more rapidly than reaction—an assumption that is a basic tenet of the theory of unimolecular decomposition. With rate coefficients as large as  $\sim 5 \times 10^{12} \text{ s}^{-1}$ , if unimolecular decomposition cannot win the competition against vibrational relaxation, it never will.

The  $\text{He}_n$  droplets are sufficiently small (i.e.,  $\langle n \rangle \sim 10\,000$ )<sup>14</sup> that we must consider the possibility that one (or even both) of the fragments exits its droplet, because the momentum it receives via dissociation has not been fully dissipated when it reaches the surface. For this to happen with droplets that consist of several thousand helium atoms, the fragment must, on average, make its way past at least half a dozen helium atoms to get to the surface, and then pass from there into the gas phase. This is not easy. After its formation, the fragment will knock about in the helium, progressively losing memory of its original momentum direction. If it fails to reach the surface with translational energy in excess of its solvation energy, it is trapped, never to leave the droplet.

This leads us to the central issue addressed in the work reported here. Do fragments, in fact, leave their droplets, and if

so, to what extent and retaining how much internal excitation and in which forms? Photoexcitation is carried out by using photon energies that range from the gas-phase dissociation threshold,  $D_0$ , to approximately  $D_0 + 4300\text{ cm}^{-1}$  (where  $k_{\text{uni}}$  is  $\sim 5 \times 10^{12}\text{ s}^{-1}$  for gas-phase NO<sub>2</sub>).  $D_0$  is chosen as a reference energy, even though we know that dissociation will not occur for photon energies at, or just above,  $D_0$  when NO<sub>2</sub> is embedded in He<sub>n</sub>.

Photoinitiated unimolecular decomposition is, notwithstanding a few details, a well-understood phenomenon for gas-phase molecules. When molecules embedded in He<sub>n</sub> are considered, however, it becomes complex. In contrast to direct photodissociation, which occurs rapidly and with considerable interfragment repulsion, the dissociation mechanism itself, even the issue of what constitutes dissociation, is intimately related to interactions of the molecular system with its helium environment. The most obvious example is the competition between vibrational relaxation and unimolecular decomposition, and even here the matter is subtle.

When there is no barrier along the reaction coordinate for the gas-phase counterpart, it is hard to define the point at which reaction has taken place in He<sub>n</sub>.<sup>15</sup> For example, with NO<sub>2</sub>, if the O–NO distance reaches, e.g., 6 Å, does that mean that reaction has occurred? In the gas phase, the answer is, except barely above threshold, where the interfragment de Broglie wavelength is huge, an unequivocal *yes*. At 6 Å, the system has evolved to the product side of the transition state.

In He<sub>n</sub>, however, the fragments may never get further apart than 6 Å, e.g., if the attractive interaction between them at 6 Å exceeds the amount of translational energy that remains after they have been slowed by their helium environment. In fact, if the fragments do not exit their cluster, it is *inevitable* that they will recombine, forming ground-state NO<sub>2</sub> or, conceivably, a metastable form that corresponds to a local minimum on the potential surface. They have no alternative; their mutual attraction, though small at large distances, overcomes their solvation energies in the liquid. Moreover, in many cases the “fragments” will not even get sufficiently far apart before their momentum is dissipated to justify calling them fragments. In consideration of the above, we believe that there can be no well-defined reaction threshold for a system whose gas-phase counterpart is unimolecular decomposition via a loose transition state.

On the other hand, a system having a significant exit channel barrier (in addition to the reaction exoergicity) will behave differently. In this case, the transition state lies near the exit barrier and it is relatively well-defined. Past this barrier, products are accelerated and they encounter the helium with momentum gained past the barrier, which can be significant. This increases the probability of products escaping from the cluster. Most importantly, they cannot recombine except to form weakly bound van der Waals species, so even if they fail to enter the gas phase, there can be a drop in the mass spectrometer depletion signal. Ultimately, it will be interesting to compare these two kinds of unimolecular reaction. Here, we examine the He<sub>n</sub> analogue of the barrierless gas-phase reaction.

### Experimental Approach and Results

The experimental arrangement shown schematically in Figure 2 has been described elsewhere, though briefly.<sup>6</sup> There are three separately pumped chambers. In the first, He<sub>n</sub> droplets are produced by expanding ultrapure helium (99.9999%, Spectra Gases) through a 5 μm diameter hole (National Aperture) that is cooled by using two closed-cycle helium refrigerators (CTI

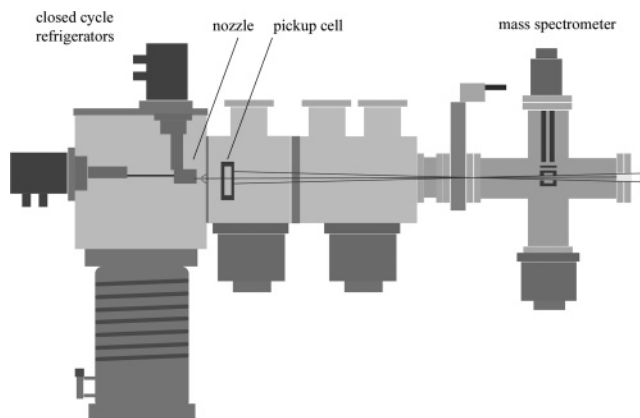


**Figure 2.** Schematic drawing of the experimental arrangement. The source chamber is evacuated with a diffusion pump. The pickup and detection chambers are evacuated with turbomolecular pumps. The laser beam (entering on the right) is collinear and counter-propagating with the molecular beam.

Cryogenics and Advanced Research Systems). The former precools the helium before it enters the nozzle assembly, whereas the latter maintains the low temperature of the nozzle itself. In the present experiments, the stagnation temperature was 14.5 K and the pressure behind the nozzle was 50 bar. The mean size of the clusters produced under these conditions is  $\langle n \rangle \sim 10\,000$ .<sup>14</sup> Temperatures were measured by using a silican diode sensor (Lakeshore) having an accuracy of  $\pm 0.5\text{ K}$ . The source chamber operating pressure is  $2 \times 10^{-4}\text{ mbar}$ .

The detection region is separated from the pickup chamber by a 5 mm diameter aperture. The background pressure in the detection region is  $\sim 10^{-8}\text{ mbar}$ , which is low enough to avoid problems that arise from contamination by impurities. A quadrupole mass spectrometer (Balzers) was used to monitor the depletion of signals arising from droplets containing NO<sub>2</sub>. The mass spectrometer was installed with its quadrupole axis perpendicular to the molecular beam axis in order that the laser beam could be overlapped with the molecular beam. The length of this interaction region is 75 cm, corresponding to the duration of the depletion signal of 2.5 ms. The electron multiplier output of the mass spectrometer was connected to a 12-bit ADC computer board (Gage Applied Sciences, CS8012) through a  $\times 10$  preamplifier that is part of the mass spectrometer system.

Optical spectra were recorded over the energy range 24 900–29 400  $\text{cm}^{-1}$  (402–340 nm) by using the mass spectrometric depletion method, which has been applied widely in studies of doped He<sub>n</sub> droplets.<sup>2</sup> It is described here briefly.

Consider a cluster that contains an embedded molecule. Electron impact excitation (i.e., which takes place in the ionizer region of the quadrupole mass spectrometer) ionizes clusters, which then decompose into a number of fragments, yielding numerous daughter ions that appear as peaks in the mass spectrum. The total number of daughter ions is proportional to the cross sectional area of the cluster, e.g.,  $\sim 70\text{ nm}^2$  for  $n = 10\,000$ . Any process that causes the cluster to become smaller will decrease the number of ions. In the simplest cases, this decrease is the “depletion” that constitutes the desired signal.

Photoexcitation that is followed by deactivation by the helium host results in evaporation. This shrinks the cluster and therefore yields a depletion signal. A good example is  $m/z = 8$ , i.e., He<sub>2</sub><sup>+</sup>. This species derives from electron impact ionization of He<sub>n</sub> clusters, and therefore it can be used to record depletion spectra. Daughter ions that contain all or part of an embedded molecule (in the present case NO<sub>2</sub>) can also be used to record spectra, though interpretation is subtler, as discussed in the next section.

In this case, the depletion strength is proportional to the amount of energy deposited into the helium degrees of freedom. The situation is more complex if photodissociation occurs, and it is possible for fragments to leave the droplet, as discussed later.

The depletion spectrum presented in this work covers the wavelength region from 340 to 402 nm. On the short-wavelength side of this region, radiation was obtained by doubling the output of a dye laser (Continuum ND6000) pumped by the second harmonic of a Nd:YAG laser (Continuum Powerlite 9020). The region 340–365 nm was covered by using the dyes DCM, LDS 698, LDS 722, and LDS 750. Energies ranged from 5 to 19 mJ, with a mean of 12.5 mJ.

Radiation from 365 to 402 nm was obtained by mixing the dye laser output with the Nd:YAG fundamental. Injection-seeding (LightWave Technologies) of the Nd:YAG laser narrows its line width, thereby increasing conversion efficiency. The following dyes were used in this region: R590; a mixture of R590 and R610; R610; a mixture of R610 and R640; R640; and DCM. The 365–402 nm energies varied from 8 to 22 mJ, with an average of 17 mJ. Wavelength calibration was achieved by recording opto-galvanic spectra prior the experiment, as described elsewhere.<sup>16</sup> Radiation was focused with a 50 cm focal length lens to avoid damaging the nozzle.

After passing through a 400  $\mu\text{m}$  diameter skimmer, the droplet beam passes through a 3 cm long pickup cell containing  $\text{NO}_2$  (Matheson, 99.5%, used without purification) that is 13 cm downstream from the skimmer.

The ratios of the numbers of droplets that contain 0, 1, 2, etc. molecules depend on pressure in the pickup cell and are governed by Poisson statistics.<sup>14</sup> The pickup process can be monitored, albeit with some uncertainty, by observing intensities of peaks in the mass spectra that correspond to  $\text{NO}_2^+$ ,  $(\text{NO}_2)_2^+$ , etc. Despite the fact that  $\text{N}_2\text{O}_4$  does not absorb in this wavelength region, we found that the depletion signal increases with pickup cell pressure. This is consistent with the formation of metastable (i.e., van der Waals type) complexes that absorb in this region, e.g.,  $\text{NO}_2\text{--NO}_2$  instead of  $\text{N}_2\text{O}_4$ . In consideration of this, the pickup cell pressure was adjusted to achieve “optimal” conditions. Namely, when the number of droplets that contain a single  $\text{NO}_2$  molecule is about 70% of its maximum value, only a few percent of the droplets contain more than one  $\text{NO}_2$  molecule. The pressure in the pickup chamber was monitored with a “micro” ion gauge (Granville-Phillips); its reading under optimal conditions was  $2.7 \times 10^{-7}$  Torr.

Care was taken to lessen experimental uncertainties over the broad spectral region examined here. At each wavelength, time dependencies of the electron multiplier outputs at  $m/z$  values of 8 ( $\text{He}_2^+$ ), 30 ( $\text{NO}^+$ ), and 46 ( $\text{NO}_2^+$ ) were recorded and results from 2000 laser firings were averaged. The laser energy was measured with a power meter (SciTech Astral, AC2501 head) located at the point where the laser beam enters the vacuum chamber, and the laser wavelength was set manually. To lessen effects that might arise from the data depending on uncontrolled parameters, and to check day-to-day repeatability, this wavelength was chosen randomly. Moreover, data in the same spectral region were recorded twice to check repeatability.

The intensity of the depletion signal was found to depend linearly on laser energy, and the data presented in Figure 3 are normalized with respect to laser energy and include  $1\sigma$  error bars. The data have not been corrected for the variation of the  $\text{NO}_2$  absorption cross section in this region; this variation is expected to be modest on the basis of measurements made at higher temperatures. Because of the broad absorption line widths (i.e.,  $\geq 7 \text{ cm}^{-1}$ , corresponding to rapid relaxation), high laser

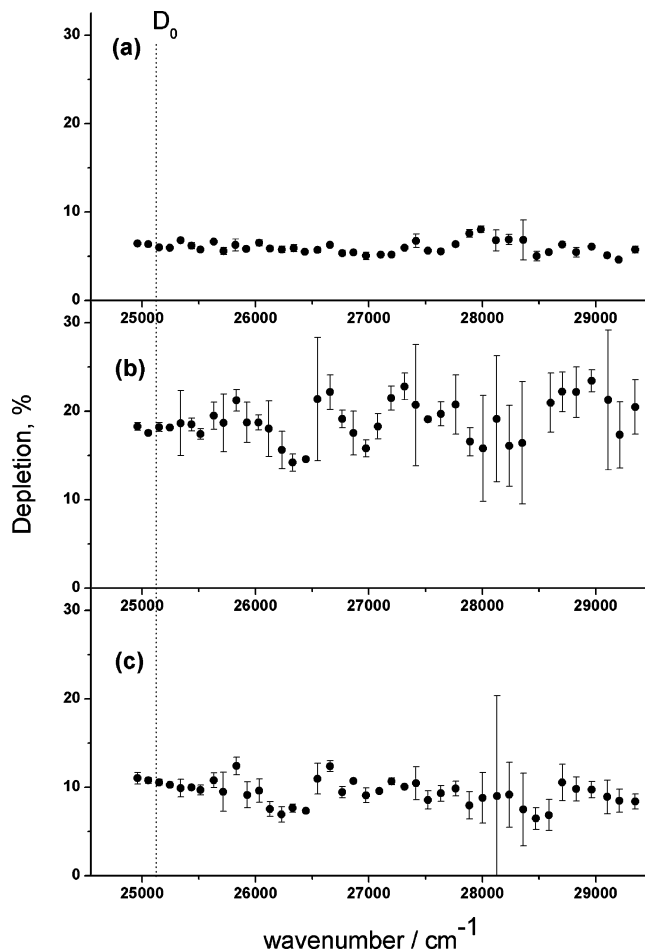


**Figure 3.** Mass spectrometer depletion spectra for  $m/z$  values of: (a) 8 ( $\text{He}_2^+$ ); (b) 46 ( $\text{NO}_2^+$ ); (c) 30 ( $\text{NO}^+$ ). When error bars are not visible, they are smaller than the points.

energies are required to achieve efficient excitation. For example, the energies used here exceed those needed to saturate the corresponding gas-phase transitions by several orders of magnitude. The data corresponding to  $m/z = 8$  are also normalized with respect to pickup cell pressure. Data were recorded at 0.25 nm intervals and subjected to a six-point smooth.

## Discussion and Conclusions

The data presented in Figure 3a for  $m/z = 8$  (i.e., monitoring  $\text{He}_2^+$ ) indicate that there is no significant change in the depletion of the  $m/z = 8$  signal as the photon energy is varied throughout its tuning range. The  $\text{He}_2^+$  ion arises from electron impact ionization of clusters, regardless of the nature of the embedded species they contain. For clusters that contain  $\text{NO}_2$ , photoexcitation of the embedded  $\text{NO}_2$  yields depletion signals, as discussed in the previous section. The size of the depletion signal (i.e.,  $\sim 7\%$  throughout the tuning range, see Figure 3a) is consistent with the degree of doping ( $\sim 26\%$  of the  $\text{He}_n$  clusters contain a single  $\text{NO}_2$  molecule) and efficient photoexcitation, which is achieved by using high-energy laser pulses. A photon energy of  $25\,000 \text{ cm}^{-1}$  is sufficient to evaporate approximately 5000 helium atoms. For  $h\nu < D_0$ , the photoexcited molecules relax to the ground state, and therefore the full photon energy is available for the evaporation of helium atoms.

When a large fraction of the photon energy is needed to break a bond, there is relatively little energy left for the evaporation of helium atoms. However, even if fragments are produced within a droplet, if they recombine, there is no net reaction.

Consequently, the full photon energy goes into heat, and the amount of evaporation is large, i.e., it is essentially identical to that which would occur without fragmentation.

The situation is quite different if one (or both) of the photofragments leaves the cluster. In this case, the depletion signal will be relatively small because most of the photon energy is used to break the bond, which *remains* broken. Thus, the constancy of the percent depletion throughout the range 24 900–29 400 cm<sup>-1</sup> indicates that there is little, if any, *net* reaction over this energy range. The photon energy goes into the evaporation of helium, and it brings about no chemical change.

Let us now consider the case of  $m/z = 46$  (i.e., monitoring NO<sub>2</sub><sup>+</sup>) shown in Figure 3b. The percent depletion is larger than that obtained by monitoring  $m/z = 8$  (i.e., ~18% versus ~7%, as shown in Figure 3b,a, respectively), in large part because the mass spectrometer signals at  $m/z = 8$  contain significant contributions from clusters that contain no NO<sub>2</sub>, and which therefore cannot contribute to the depletion signal. For cases in which dissociation results in one or both fragments leaving the droplet, the NO<sub>2</sub><sup>+</sup> mass spectrometer signal vanishes, yielding the largest possible depletion signal. If neither fragment leaves the droplet, the NO<sub>2</sub><sup>+</sup> mass spectrometer signal diminishes significantly—but it does not vanish—because all of the photon energy contributes to shrinkage of the droplet. For a cluster containing 10 000 helium atoms, the number of helium atoms that evaporate for photon energies in the range 24 900–29 400 is roughly 5000–6000, and the cross sectional area is reduced to ~60% of its original value. Thus, the data shown in Figure 3b—namely, the fact that there is no discernible change over the photon energy tuning range—indicate that fragments do not leave their cluster to any significant degree. This is consistent with the data shown in Figure 3a.

Figure 3c shows the variation of the mass spectrometer depletion signal obtained at  $m/z = 30$  (i.e., monitoring NO<sup>+</sup>). If dissociation causes an oxygen atom to leave the cluster, with NO remaining in the cluster, the depletion signal will diminish but only slightly. If, on the other hand, NO leaves the cluster, either by itself or with a modest number of helium atoms attached, the amount of depletion will be significant. Because the oxygen atom receives 65% of the center-of-mass translational energy, and because it is smaller than NO, it will have an easier time exiting the cluster than would NO. Consequently, the  $m/z = 30$  signal will *increase*, because shrinkage of the cluster is modest, whereas NO<sup>+</sup> is now a primary ion, rather than a daughter ion that derives from NO<sub>2</sub>. The constancy observed in Figure 3c therefore is consistent with there being no net reaction, in accord with the other data. The signal at  $m/z = 30$  contains contributions from the wings of the strong peaks at  $m/z = 28$  (N<sub>2</sub><sup>+</sup>) and  $m/z = 32$  (O<sub>2</sub><sup>+</sup>); this is why depletion at  $m/z = 30$  is less than that at  $m/z = 46$ .

The data presented in the previous section show that, to within the experimental uncertainty, there is no net photoinitiated reaction over the 4300 cm<sup>-1</sup> energy range that extends upward from  $D_0$ . The experiments do not provide direct information about the intracluster dynamics of photoexcited NO<sub>2</sub> interacting with its environment. They do, however, show that fragments do not, to any significant extent, leave the He<sub>n</sub> clusters and pass into the gas phase. Nor do the fragments reunite to an appreciable extent in the form of metastable species—akin to the phenomenon that occurs with molecules such as HCN, which forms linear chains in preference to lower energy structures.<sup>17</sup>

The failure of this system to react in the energy region just above  $D_0$  has been reported by Lehmann and co-workers,<sup>18</sup> who examined energies as high as several hundred cm<sup>-1</sup> above  $D_0$ .

At these energies,  $k_{\text{uni}}$  values are  $\leq 5 \times 10^{11} \text{ s}^{-1}$ .<sup>13,19</sup> On the basis of the broad line widths seen in Figure 1 (which were not available at the time of the measurements of Lehmann and co-workers), it is clear that reaction in this energy regime is unlikely, as  $k_{\text{uni}}$  is at least several times smaller than the deactivation rates. Even if the average energy that is lost upon the deactivation of a given level is modest,  $k_{\text{uni}}$  drops from  $4 \times 10^{11} \text{ s}^{-1}$  at  $E - D_0 = 200 \text{ cm}^{-1}$  to  $<10^{11} \text{ s}^{-1}$  just above  $D_0$ , making reaction progressively less likely as  $E$  decreases.

Most importantly, at these small energies in excess of  $D_0$ , fragments cannot escape the immediate confines afforded by the surrounding helium, and *net* reaction is out of the question. The fact that the formation of a metastable NO–O species does not occur to an appreciable extent is consistent with our understanding of NO<sub>2</sub> intramolecular dynamics near  $D_0$ , because the long-range potential supports NO rotation relative to the oxygen atom, as evidenced by the efficient production of low NO rotational levels just above  $D_0$ , in accord with statistical theory.<sup>15,20</sup>

In the current study, the energy in excess of  $D_0$  has been varied from zero to 4300 cm<sup>-1</sup>. At the upper end of this range,  $k_{\text{uni}}$  is  $\sim 5 \times 10^{12} \text{ s}^{-1}$ , which is as large a rate coefficient as is possible for a system that reacts via a unimolecular decomposition mechanism. Consequently, NO<sub>2</sub> serves as a benchmark example of the photoexcitation of an embedded small polyatomic whose gas-phase counterpart undergoes a barrierless reaction. Its rate coefficient can be increased easily to the maximum value possible, and relaxation in the regime of quantum chaos has been measured for resolved levels, due to the modest density of vibronic levels.

For the largest  $k_{\text{uni}}$  values ( $\sim 5 \times 10^{12} \text{ s}^{-1}$ ), it is likely that in He<sub>n</sub> the O–NO distance increases beyond the loose transition-state region for the corresponding gas-phase reaction; i.e., the molecule comes apart. This conjecture is based on the fact that  $k_{\text{uni}}$  is at least as large as, and probably larger than, the rate of deactivation. The system then recombines, as it must as long as it remains within the droplet, whose liquidity guarantees recombination. Were the photoexcited moiety in a solid matrix, products could be isolated.

The fact that net reaction has not been observed in this system leads us to the conclusion that no photoexcited polyatomic molecule will undergo barrierless unimolecular decomposition in He<sub>n</sub> droplets of sizes similar to the ones used here, with two possible exceptions. First, a product with a positive chemical potential inside the droplet will be expelled, as with alkali atoms. Second, a small cross section for collision of a product with a helium atom, as with atomic hydrogen, enhances the escape probability.

Finally, we note that reaction is assured with small droplets. For example, 4300 cm<sup>-1</sup> is sufficient to evaporate  $\sim 10^3$  atoms. Thus, with  $\langle n \rangle \sim 10^3$ , a significant fraction of the clustered helium will evaporate completely, leaving gas-phase NO<sub>2</sub> with  $E > D_0$ .

**Acknowledgment.** We have benefited from numerous scientific discussions with Andrey Vilesov. This research has been supported by the U.S. National Science Foundation (CHE-0203978).

## References and Notes

- (1) Stienkemeier, F.; Vilesov, A. *J. Chem. Phys.* **2001**, *115*, 10119.
- (2) Toennies, J.; Vilesov, A. *Annu. Rev. Phys. Chem.* **1998**, *49*, 1.
- (3) Nauta, K.; Moore, D.; Miller, R. *Faraday Discuss. Chem. Soc.* **1999**, *113*, 261.

- (4) Hartmann, M.; Mielke, F.; Toennies, J.; Vilesov, A. *Phys. Rev. Lett.* **1996**, *76*, 4560.
- (5) Lugovoj, E.; Toennies, J.; Vilesov, A. *J. Chem. Phys.* **2000**, *112*, 8217.
- (6) Polyakova, E.; Stolyarov, D.; Zhang, X.; Kresin, V. V.; Wittig, C. *Chem. Phys. Lett.* **2003**, *375*, 253.
- (7) Georges, R.; Delon, A.; Jost, R. *J. Chem. Phys.* **1995**, *103*, 1732.
- (8) Delon, A.; Jost, R.; Lombardi, M. *J. Chem. Phys.* **1991**, *95*, 5701.
- (9) Callegari, C.; Lehmann, K.; Schmied, R.; Scoles, G. *J. Chem. Phys.* **2001**, *115*, 10090–10110.
- (10) Jost, R.; Nygard, J.; Pasinski, A.; Delon, A. *Phys. Rev. Lett.* **1997**, *78*, 3093.
- (11) Drabbels, M. Imaging the Photodynamics of Molecules in Liquid Helium Droplets. International Symposium on Stereodynamics of Chemical Reactions, 2002, Alkmaar, The Netherlands.
- (12) Kanaev, A. V.; Museur, L.; Laarmann, T.; Monticone, S.; Castex, M. C.; von Haefen, K.; Moller, T. *J. Chem. Phys.* **2001**, *115*, 10248.
- (13) Ionov, S. I.; Brucker, G. A.; Jaques, C.; Chen, Y.; Wittig, C. *J. Chem. Phys.* **1993**, *99*, 3420.
- (14) Lewerenz, M.; Schilling, B.; Toennies, J. P. *J. Chem. Phys.* **1995**, *102*, 8191.
- (15) Reid, S. A.; Reisler, H. *J. Phys. Chem.* **1996**, *100*, 474.
- (16) Zhu, X.; Nur, A.; Misra, P. *J. Quant. Spectrosc. Radiat. Transfer* **1994**, *52*, 167.
- (17) Nauta, K.; Miller, R. E. *Science* **1999**, *283*, 1895.
- (18) Lehmann, K. *Faraday Discuss. Chem. Soc.* **2001**, *118*, 55.
- (19) Stolyarov, D.; Polyakova, E.; Bezel, I.; Wittig, C. *Chem. Phys. Lett.* **2002**, *358*, 71.
- (20) Reid, S. A.; Brandon, J. T.; Hunter, M.; Reisler, H. *J. Chem. Phys.* **1993**, *99*, 4860.